DR FAREEDA ATHAR (Orcid ID : 0000-0002-6566-7573)

DR OBAID AFZAL (Orcid ID : 0000-0002-4188-5592)

Article type : Research Article

Pyrrolidin-2-one Linked Benzofused Heterocycles as Novel Small Molecule Monoacylglycerol Lipase Inhibitors and Antinociceptive Agents

Running title: Pyrrolidin-2-one derivatives as MAGL inhibitors.

Abdulmalik Saleh Alfawaz Altamimi[1], Sandhya Bawa[2], Fareeda Athar[3], Md Quamrul Hassan[4], Yassine Riadi[1], Obaid Afzal[1*]

[1] Department of Pharmaceutical Chemistry, College of Pharmacy, Prince Sattam Bin Abdulaziz University, AlKharj-11942, Saudi Arabia.

[2] Department of Pharmaceutical Chemistry, School of Pharmaceutical Education and Research, Jamia Hamdard, New Delhi-110062, India.

[3] Centre for Interdisciplinary Research in Basic Sciences, Jamia Millia Islamia, New Delhi-110025, India.

[4] Department of Pharmacology, School of Pharmaceutical Education and Research, Jamia Hamdard, New Delhi-110062, India.

*** Corresponding author**

Obaid Afzal (Ph.D.)

Assistant Professor
Department of Pharmaceutical Chemistry
College of Pharmacy
Prince Sattam Bin Abdulaziz University
AlKharj-11942, Saudi Arabia.
Tel.: +966115886094, Mob.: +966544322364
E-mail: obaid263@gmail.com; o.akram@psau.edu.sa

Abstract

Eighteen pyrrolidin-2-one linked benzothiazole, and benzimidazole derivatives (**10-27**) were designed and synthesized. The structure of the compounds was confirmed by elemental and spectral (IR, ^{1}H-NMR, and MS) data analysis. All the compounds were screened by human monoacylglycerol lipase (*h*MAGL) inhibition assay. Three benzimidazole compounds, **22** (4-Cl phenyl), **23** (3-Cl,4-F phenyl), and **25** (4-methoxy phenyl) were found to be the most potent, having an IC_{50} value of 8.6 nM, 8.0 nM and 9.4 nM, respectively. Among them, the halogen-substituted phenyl derivatives, compound **22** (4-Cl phenyl) and compound **23** (3-Cl,4-F phenyl), showed micromolar potency against fatty acid amide hydrolase (FAAH), having an IC_{50} value of 35 μM and 24 μM, respectively. Benzimidazole derivative having 4-methoxyphenyl substitution (compound **25**) was found to be a selective MAGL inhibitor (IC_{50} = 9.4 nM), with an IC_{50} value above 50 μM against FAAH. In the formalin-induced nociception test, compound **25** showed a dose-dependent reduction of pain response in both acute and late phases. At 30 mg/kg dose, it

significantly reduced the pain response and showed greater potency than the reference drug gabapentin (GBP).

Keywords

Pyrrolidin-2-one; Benzothiazole; Benzimidazole; MAGL inhibitors; Pain

1. Introduction

2-Arachidonoylglycerol (2-AG) and *N*-arachidonoylethanolamine (AEA; Anandamide) are bioactive lipids (major endocannabinoids), released upon cell membrane activation. Their functions are mediated by the stimulation of two G-protein-coupled receptors, CB_1 and CB_2 (cannabinoid receptors). Moreover, 2-AG and AEA have also been identified to act on several other receptors like transient receptor potential vanilloid (TRPV1) and peroxisome proliferator activated receptors (PPARs) [1-4]. 2-AG (major endocnnabinoid) and AEA are hydrolysed by the enzymes monoacylglycerol lipase (MAGL) and fatty acid amide hydrolase (FAAH), respectively [5]. MAGL is an α/β-hydrolase enzyme that catalyses 2-AG into free fatty acid (FFA) and glycerol via a catalytic triad (Ser122, Asp239 and His269) [6]. MAGL has been suggested to be the main α/β-hydrolase that terminates 2-AG actions in the central nervous system (CNS), contributing

~85% of total 2-AG hydrolysis. Residual ~15% of 2-AG is stated to be hydrolysed by α/β-hydrolase domain (ABHD)-containing proteins (ABHD6 and ABHD12) [7].

The hydrolysis of 2-AG generates arachidonic acid (AA), which acts as the precursor for the production of inflammatory prostaglandins (PGE_2 and PGD_2) by COX-dependent mechanism. In the brain, 2-AG hydrolysis was shown to provide the principal source of the neuro-inflammatory prostaglandins. The inhibition of MAGL has exerted substantial anti-inflammatory and neuroprotective properties in animal models of Alzheimer's and Parkinson's disease [8,9]. MAGL inhibitors are reported to increase 2-AG levels in the CNS and consequently caused weakened mechanical and cold allodynia, by the action of 2-AG on CB_1 receptors, founding their ability to reduce neuropathic pain [10,11]. The role of 2-AG in neuropathic pain has been comprehensively documented. It has been suggested that 2-AG exhibits antinociception by acting both in the CNS and the periphery [12-15]. JJKK-048 (MAGL, IC_{50} 363 pM) is a potent and selective MAGL inhibitor and appeared to be extremely potent *in vivo*. JJKK-048 causes a considerable surge of 2-AG levels without affecting AEA levels in mouse brain. It has been shown that JJKK-048 caused significant analgesia in a writhing test and tail immersion test, without any notable cannabimimetic side effects [16]. Thus, MAGL inhibitors are potentially useful for the treatment of pain, inflammation, and CNS disorders. The interesting findings advocated that MAGL inhibition convene significant therapeutic benefits in neurological disorders and neuropathic pain [17-19].

SAR629 and congeners (a triazolo carboxamide) were discovered as potent dual MAGL-FAAH inhibitors. The crystal structure of the MAGL inbound with the inhibitor SAR629 was also reported [20]. ML30 has been reported to be a potent (IC_{50} 0.54 nM) human MAGL inhibitor with a 1,000-fold selectivity versus FAAH [21]. In agreement, Aaltonen et al. observed a similar potency for ML30 (IC_{50} 1.5 nM) toward hMAGL. Both compounds, JJKK-048 and KML29 exhibited outstanding MAGL selectivity over FAAH (>10,000-fold) [22,23]. The comprehensive description of the active site of MAGL was revealed by X-ray diffraction method (Protein Data Bank, PDB ID: 3HJU), at 2.2 Å resolution [24]. Another X-ray crystal structure of *h*MAGL bound with the inhibitor ZYH was determined recently with the use of molecular replacement method to a resolution of 1.35 Å (PDB ID: 3PE6) [25]. A detailed explanation of the crystal structure of MAGL and its inhibitors was published recently [26]. Based on the promising therapeutic benefits of MAGL inhibitors, Abide Therapeutics (California, United States) announces the clinical study

of ABX-1431, which is currently in clinical trials for neurological disorders [27]. Moreover, PF-06795071 (a trifluoromethyl glycol carbamate derivative) was discovered by Pfizer (Massachusetts, United States), as a potent and selective covalent MAGL inhibitor (IC_{50} = 3 nM) for the treatment of neuro-inflammation [28]. Takeda Pharmaceuticals Co. Ltd. (Kanagawa, Japan) identified a potent and reversible MAGL inhibitor (IC_{50} = 3.6 nM), comprising of piperazinyl linked pyrrolidin-2-one moiety (Compound 23, Figure 1). The coordinates of the crystal structures of MAGL in complex with a piperazinyl pyrrolidin-2-one derivative (PDB ID: 5ZUN) have also been reported [29]. A benzoylpiperidine derivative (compound 23, IC_{50} = 80 nM) is reported as potent and selective reversible MAGL inhibitor [30]. A benzisothiazolinone (BTZ) derivative (Compound 13, Figure-1) has been revealed recently as MAGL inhibitor (IC_{50} = 34.1 nM), targeting allosteric regulatory cysteine residues (Cys201 and Cys208) [31]. Our group have identified two novel human MAGL inhibitors, ZINC24092691 (IC_{50} = 10 nM) and ZINC12863377 (IC_{50} = 39 nM) by docking based virtual screening of ZINC database. Furthermore, the structure-activity relationship study of ZINC24092691 lead to a derivative having an IC_{50} value of 6.5 nM [32,33]. The structures of potent MAGL inhibitors, along with their IC_{50} values, are presented in **Figure 1**.

The MAGL active site comprises three parts; viz. (a) a hydrophobic void for bulky fatty acid chain of 2-AG, (b) nucleophilic elbow/oxyanion hole, consisting critical amino acid residues, Ser122, Ala51, and Met123, where the formation of H-bonds or covalent bonds in the catalytic site of the enzyme takes place and (c) a small amphiphilic pouch/space for the exiting group glycerol. Bearing in mind, the possibility of structural modification in the MAGL native substrate (2-AG) and the binding configuration of MAGL inhibitors, ZINC12863377 (IC_{50} = 39 nM) and ZINC24092691 (IC_{50} = 10 nM), novel small molecules MAGL inhibitors (**10-27**) were designed (**Figure-2**). All the designed and synthesized compounds were assayed for their human MAGL inhibitory potential. To find selective inhibitors, the most potent compounds were further assayed against human FAAH. The most potent and selective MAGL inhibitor was then evaluated for their antinociceptive activity on formalin-induced hyperalgesia.

2. Results and discussion

The binding pattern of ZINC24092691 (IC_{50} = 10 nM) and ZINC12863377 (IC_{50} = 39 nM), at the active site of MAGL protein, was used to design novel small molecule MAGL inhibitors (**10-27**). Their design and route of synthesis are depicted in **Figure 2** and **Figure 3**, respectively.

2.1. Chemistry

1-(substituted phenyl)-5-oxopyrrolidine-3-carboxylic acids (**1-9**) were synthesized by direct condensation of appropriate anilines and itaconic acid (methylene succinic acid) at their fusion point, as reported in the literature [34]. The condensation of the terminal carboxylic group in compounds 1-9 with 2-aminobenzenethiol or 1,2-diaminobenzene was carried out with some modification in the procedure reported earlier [35]. The condensation was driven by polyphosphoric acid, which gives us better yield and purity of benzothiazole (**10-18**) and benzimidazole derivatives (**19-27**). Based on the generated elemental and spectral (infra-red spectroscopy, nuclear magnetic resonance spectroscopy, and mass spectrometry) data, the structure of the compounds was confirmed.

In the IR spectrum of compound **1** (1-Phenyl-5-oxopyrrolidine-3-carboxylic acid), the characteristic absorption bands at 3252 cm^{-1}, 1734 cm^{-1}, and 1692 cm^{-1} were attributed to the O-H of carboxylic acid, C=O of pyrrolidine ring and C=O of carboxylic acid, respectively. The ^{1}H-NMR spectrum of compound **1** exhibited a characteristic singlet at δ 11.79 due to the presence of –COOH proton, which is D_2O exchangeable. The doublet appearing at δ 7.65-7.62 (J = 9 Hz) was assigned to two ortho proton of the phenyl ring, while two triplets at δ 7.39-7.34 (J = 7.5 Hz) and δ 7.16-7.11 (J = 7.2 Hz), were attributed to two meta and one para proton of the phenyl ring, respectively. The multiplet resonating at δ 4.08-3.93 was assigned to two NCH_2 and one CH proton of the pyrrolidin-2-one ring, while the other two $COCH_2$ protons of the pyrrolidin-2-one ring appeared as a multiplet at δ 2.80-2.65. The spectral data of compound **10** (benzothiazole derivative having unsubstituted phenyl) exhibits specific IR bands at 1691 cm^{-1} and 1602 cm^{-1}, due to the presence of C=O bond of the pyrrolidin-2-one ring and C=N function of the benzothiazole ring, respectively. In the ^{1}H-NMR spectrum of compound **10**, all the nine aromatic protons of benzothiazole and phenyl ring appeared resonating at δ 8.17-7.15 as multiplet. The multiplet resonating at δ 4.39-4.17 was assigned to two NCH_2 and one CH proton of the pyrrolidin-2-one ring, while the other two $COCH_2$ protons of the pyrrolidin-2-one ring appeared as a multiplet at δ 3.19-2.97. Moreover, the mass spectrum of compound **10** showed the molecular ion peak, i.e., m/z (M^+) at 294.10, which confirmed its successful synthesis. The IR spectrum of compound **19** (benzimidazole derivative having unsubstituted phenyl) showed stretching bands at

3387 cm^{-1}, 1695 cm^{-1}, and 1592 cm^{-1}, due to the characteristic N-H of benzimidazole, C=O of pyrrolidine, and C=N of benzimidazole, respectively. In the ^1H NMR spectrum of compound **19**, the broad singlet appearing at δ 12.48 showed the presence of D_2O exchangeable N-H proton. Two protons of benzimidazole (H-4 and H-7) appeared as a doublet at δ 7.69-7.67 (*J* = 8.1 Hz). Remaining seven aromatic protons of benzimidazole and phenyl ring appeared as a multiplet at δ 7.52-7.36 and δ 7.17-7.12. Three multiplets, resonating between δ 4.32-4.19, δ 4.05-3.95, and δ 3.10-2.93, were assigned to two NCH_2, one CH and two $COCH_2$ protons of the pyrrolidin-2-one ring. The mass spectrum of the compound **19**, having *m/z* 277.15 (M^+), further confirmed its successful synthesis.

2.2. In vitro hMAGL enzyme inhibition assay

The hMAGL enzyme inhibition assay was done with the method reported previously using Cayman's assay kit [33,36]. All the eighteen compounds (10-27) were screened for their ability to inhibit MAGL protein. Overall, the benzimidazole linked pyrrolidin-2-one derivatives (19-27) showed better activity than their benzothiazole analogs (10-18). Three compounds (22, 23, and 25) were found to decrease the MAGL activity below 50 % at 10 nM concentration. Among them, the halogen-substituted phenyl derivatives, compound 22 (4-Cl phenyl) and compound 23 (3-Cl,4-F phenyl) were found to be most potent, having an IC_{50} value of 8.6 nM and 8.0 nM, respectively. Also, compound 25 (4-methoxy phenyl) was almost equipotent as their halogen-substituted counterparts, with an IC_{50} value of 9.4 nM. The structure-activity relationship (SAR) of benzimidazoles derivatives showed their MAGL inhibitory potential as follows: 3-Cl,4-F > 4-Cl > 4-OCH_3 > 2-CH_3 > 4-CH_3 > H > 4-NO_2 > 4-OH > 4-SO_2NH_2. The IC_{50} of standard control, a selective MAGL inhibitor, CAY10499 (IC_{50} = 415 nM) was found to be comparable as reported in literature (IC_{50} = 350 nM) [36]. The results of the *h*MAGL inhibition assay are provided in **Table 1**.

2.3. In vitro hFAAH enzyme inhibition assay

MAGL inhibitors having an IC_{50} value less than 10 nM (compound **22**, **23**, and **25**) were selected for the inhibition assay against a closely related hydrolase, FAAH [37]. Among them, the halogen-substituted phenyl derivatives, compound **22** (4-Cl phenyl) and compound **23** (3-Cl,4-F phenyl) showed micromolar potency against FAAH, having an IC_{50} value of 35 μM and 24 μM, respectively. Surprisingly, the benzimidazoles derivative having 4-methoxyphenyl substitution (compound **25**) was found to be a selective MAGL inhibitor (IC_{50} = 9.4 nM), with FAAH, IC_{50} value more than 50 μM. The IC_{50} of a selective FAAH inhibitor, URB597 (standard control), was

found to be 5 nM, comparable as reported in literature (IC_{50} = 4.6 nM) [38]. The results of the *h*FAAH inhibition assay are provided in **Table 1**.

2.4. Computational studies

2.4.1. Molecular docking

To gain insights into the binding pattern of compound 25, it was docked into the active site of MAGL protein (PDB ID: 5ZUN, Resolution-1.35 Å), by Glide XP docking using Maestro GUI of Schrodinger. The binding pose of compound 25 showed that the carbonyl function of pyrrolidin-2-one is positioned into the oxyanion hole, forming three prominent hydrogen bonds (~ 2Å) with critical amino acid residues; Ala51, Met123, and catalytic Ser122. The benzimidazole moiety is projected into the amphiphilic pocket, forming π-π stacking interaction with Tyr194. However, the 4-methoxy phenyl part of the ligand is involved in close van der Waals interactions in the hydrophobic atmosphere of Leu148, Leu213, and Leu241. 3D and 2D representation of the binding pose of compound 25 into the active site of MAGL is presented in Figure-4.

2.4.2. Physicochemical and pharmacokinetic properties

To develop a potent, selective, and orally active MAGL inhibitor, that can efficiently cross the blood-brain barrier (BBB), we analysed thirty-five physicochemical and pharmacokinetic properties of the three potent compounds having MAGL IC_{50} value less than 10 nM (compounds **22**, **23** and **25**) with the QikProp module of Schrodinger. Ghose et al. derived a guideline for the selection and optimization of CNS compounds, through the analysis of thirty-five physicochemical and pharmacokinetic properties of 317 CNS and 626 non-CNS oral drugs [40]. The guidelines for designing high-quality CNS drugs are: (i) TPSA <76 $Å^2$ (25-60 $Å^2$), (ii) no. of N atoms = 1 to 2, including one aliphatic amine), (iii) 2 to 4 linear chains outside rings, (iv) no. of polar H atoms <3 (0-1), (v) molecular volume = 740-970 $Å^3$, (vi) SASA = 460-580 $Å^2$, and (vii) a positive QikProp CNS activity parameter. Interestingly, the physicochemical and pharmacokinetic profile of compounds **22**, **23**, and **25**, was found to be within the limits as proposed and presented in the table in supplementary material.

2.5. Antinociceptive activity

2.5.1. Formalin-induced nociception test

The formalin-induced test is considered a widely accepted animal pain model. The behavioural responses to formalin consist of two distinctive phases I and II. Phase-I is an acute pain of intense licking and biting of injected paw, which lasts up to 5 minutes of formalin injection, and reflects the activity of C-fiber afferent nociceptors. Phase II reflects the state of central sensitization of the

spinal dorsal horn neurons and involves periods of licking and biting, which peaks from 10-30 minutes of formalin injection, but lasts up to 60 minutes [41,42]. Compound 25 was administered orally, 4 hours before formalin injection, at concentrations of 5, 10, 30, and 50 mg/kg, suspended in 0.5% methylcellulose. Gabapentin (GBP), a drug used in neuropathic pain, was used as a reference drug (100 mg/kg, i.p, dissolved in 0.9% normal saline). The duration of paw licking and biting during phases I and II are presented as mean±SEM in Figure 5. GBP showed only a limited effect on acute nociceptive responses (phase I), as compared to control. However, it showed a significant suppression of paw licking during phase II, confirming its central effect. Compound 25 showed a dose-dependent reduction of pain response in both acute and late phases, indicating its peripheral as well as central effect. At 30 mg/kg dose, it significantly reduced the pain response and showed greater potency than the reference drug, gabapentin (Figure 5).

3. Summary and conclusion

Pyrrolidin-2-one linked benzothiazole and benzimidazole derivatives (**10-27**) were designed as per the structural requirements of MAGL inhibitors and based on previously identified compounds reported by our group [32, 33]. All the designed compounds were successfully synthesized and characterized. Compounds (**10-27**) were screened for their potential to inhibit *h*MAGL. Three benzimidazole compounds, **22** (4-Cl phenyl), **23** (3-Cl,4-F phenyl), and **25** (4-methoxy phenyl) were found to be the most potent, having an IC_{50} value of 8.6 nM, 8.0 nM and 9.4 nM, respectively. Among them, halogen-substituted phenyl derivatives, compound **22** (4-Cl phenyl) and compound **23** (3-Cl,4-F phenyl), showed micromolar potency against FAAH, having an IC_{50} value of 35 μM and 24 μM respectively. The benzimidazoles derivative having 4-methoxyphenyl substitution (compound **25**) was found to be a selective MAGL inhibitor (IC_{50} = 9.4 nM), with an IC_{50} value of more than 50 μM against FAAH. In molecular docking analysis, the binding pattern of compound **25** showed that the carbonyl function of pyrrolidin-2-one is positioned into the oxyanion hole, forming three prominent hydrogen bonds (~ 2Å) with critical amino acid residues: Ala51, Met123, and catalytic Ser122. The benzimidazole moiety is projected into the amphiphilic pocket, forming π-π stacking interaction with Tyr194. However, the 4-methoxy phenyl part of the ligand is involved in close van der Waals interactions in the hydrophobic atmosphere of Leu148, Leu213, and Leu241. This pattern of binding is in full agreement with the inhibitor bound crystal structures reported earlier [20, 24, 26, 29]. In the formalin-induced nociception test, compound 25 showed a dose-dependent reduction of pain response in both acute and late phases. At 30 mg/kg

dose, it significantly reduced the pain response and showed higher potency than the reference drug, gabapentin (GBP). Recently, MAGL inhibitors (ABX-1431, Abide Therapeutics, USA, and PF-06795071, Pfizer, USA) were discovered and are currently under clinical trials for neurological disorders and neuropathic pain [27, 28]. Moreover, compound **25**, is a potential lead compound for further exploitation at position 1 and 4 of the pyrrolidin-2-one moiety for the development of more potent MAGL inhibitors. In conclusion, the present study confirmed that pharmacological inhibition of enzyme MAGL might convene significant therapeutic benefits in neurological disorders and neuropathic pain.

4. Experimental

4.1. Chemistry

Chemicals and reagents were purchased from Sigma Aldrich (New Delhi, India), Merck Ltd., (New Delhi, India) and S. D. Fine Chemicals Ltd. (New Delhi, India). Thin-layer chromatography (TLC) was used to assess the progress of the reaction and purity of the compounds. Melting points (M.P.) of the synthesized compounds were obtained and uncorrected by using open capillary tubes on a melting point apparatus. Elemental analysis was performed on the CHNOS-Elemental analyzer (Vario EL III) using sulphanilic acid as standard and tungsten (VI) oxide as combusting agent. Sample for analysis was prepared in Tin boats of dimension 6×6×12 mm. Infra-red (IR) spectrum was recorded by Shimadzu FT-IR spectrometer from 4000-400 cm^{-1} range, by using KBr (potassium bromide) pellets of the synthesized compounds. Bruker 300 MHz NMR instrument is used for the recording of the ^{1}H-NMR spectrum of compounds in solvent $CDCl_3$ or DMSO-d_6. UPLC–MS (Q-TOF-ESI) (Waters Corp., USA) with an ESI technique was used for molecular mass detection (m/z) of the synthesized compounds.

*4.1.1. General procedure for the synthesis of 1-(substitutedphenyl)-5-oxopyrrolidine-3-carboxylic acids (**1-9**)*

To substituted aniline (20 mmol), an equimolar amount of itaconic acid (20 mmol, 2.6 g) was added and the temperature of the reaction mixture was raised till their fusion point. After 30 minutes of stirring, mixture was cooled and chilled in an ice bath. The obtained solid was dissolved in 10% aqueous NaOH solution, treated with activated charcoal and filtered. The filtrate was acidified with dil. HCl. The resulting precipitate was filtered, washed with water and recrystallized from methanol.

4.1.1.1. 1-Phenyl-5-oxopyrrolidine-3-carboxylic acids (1)

White solid; Yield: 87 %; M.P.: 190-191 ºC; IR (KBr, cm^{-1}): 3252 (COO-H), 3045 (Ar C-H), 1734 (C=O), 1692 (C=OOH), 1522 (C=C); ^{1}H NMR (DMSO-d_6, 300 MHz) δ (ppm): 11.79 (s, 1H, COOH, D_2O exchangeable), 7.65-7.62 (d, 2H, H-2 & H-6, J = 9 Hz), 7.39-7.34 (t, 2H, H-3 & H-5, J = 7.5 Hz), 7.16-7.11 (t, 1H, H-4, J = 7.2 Hz), 4.08-3.93 (m, 3H, NCH_2 & CH_{pyrr}), 2.80-2.65 (m, 2H, $COCH_2$); ESI-MS (m/z): 205.11 (M^+); Anal. calcd. For $C_{11}H_{11}NO_3$: C, 64.38; H, 5.40; N, 6.83. Found: C, 64.44; H, 5.47; N, 6.91.

4.1.1.2. 1-(2-Methylphenyl)-5oxopyrrolidine-3-carboxylic acids (2)

White solid; Yield: 63 %; M.P.: 153-154 ºC; IR (KBr, cm^{-1}): 3243 (COO-H), 3048 (Ar C-H), 1741 (C=O), 1711 (C=OOH), 1605 (C=C); ^{1}H NMR (DMSO-d_6, 300 MHz) δ (ppm): 11.18 (s, 1H, COOH, D_2O exchangeable), 7.55-7.18 (m, 3H, H-3, H-4 & H-5), 7.10-7.05 (d, 1H, H-6, J = 7.2 Hz), 4.06-3.91 (m, 3H, NCH_2 & CH_{pyrr}), 2.82-2.64 (m, 2H, $COCH_2$); ESI-MS (m/z): 219.12 (M^+); Anal. calcd. For $C_{12}H_{13}NO_3$: C, 65.74; H, 5.98; N, 6.39. Found: C, 65.82; H, 6.00; N, 6.47.

4.1.1.3. 1-(4-Methylphenyl)-5oxopyrrolidine-3-carboxylic acids (3)

White solid; Yield: 85 %; M.P.: 186-187 ºC; IR (KBr, cm^{-1}): 3261 (COO-H), 3056 (Ar C-H), 1726 (C=O), 1695 (C=OOH), 1592 (C=C); ^{1}H NMR (DMSO-d_6, 300 MHz) δ (ppm): 11.23 (s, 1H, COOH, D_2O exchangeable), 7.52-7.49 (d, 2H, H-3 & H-5, J = 8.1 Hz), 7.18-7.15 (d, 2H, H-2 & H-6, J = 8.1 Hz), 4.05-3.90 (m, 3H, NCH_2 & CH_{pyrr}), 2.81-2.62 (m, 2H, $COCH_2$), 2.27 (s, 3H, CH_3); ESI-MS (m/z): 219.12 (M^+); Anal. calcd. For $C_{12}H_{13}NO_3$: C, 65.74; H, 5.98; N, 6.39. Found: C, 65.83; H, 6.02; N, 6.45.

4.1.1.4. 1-(4-Chlorophenyl)-5oxopyrrolidine-3-carboxylic acids (4)

White solid; Yield: 85 %; M.P.: 151-152 ºC; IR (KBr, cm^{-1}): 3245 (COO-H), 3037 (Ar C-H), 1743 (C=O), 1698 (C=OOH), 1577 (C=C); ^{1}H NMR (DMSO-d_6, 300 MHz) δ (ppm): 11.95 (s, 1H, COOH, D_2O exchangeable), 7.70-7.67 (d, 2H, H-3 & H-5, J = 9 Hz), 7.43-7.40 (d, 2H, H-2 & H-6, J = 8.7 Hz), 4.08-3.93 (m, 3H, NCH_2 & CH_{pyrr}), 2.84-2.66 (m, 2H, $COCH_2$); ESI-MS (m/z): 239.06 (M^+), 241.06 ($M^+ + 2$); Anal. calcd. For $C_{11}H_{10}ClNO_3$: C, 55.13; H, 4.21; N, 5.84. Found: C, 55.19; H, 4.29; N, 5.92.

4.1.1.5. 1-(3-Chloro-4-fluorophenyl)-5oxopyrrolidine-3-carboxylic acids (5)

White solid; Yield: 82 %; M.P.: 143-144 ºC; IR (KBr, cm^{-1}): 3289 (COO-H), 3081 (Ar C-H), 1737 (C=O), 1702 (C=OOH), 1561 (C=C); ^{1}H NMR (DMSO-d_6, 300 MHz) δ (ppm): 11.57 (s, 1H, COOH, D_2O exchangeable), 7.96-7.93 (q, 1H, H-5), 7.61-7.56 (m, 1H, H-2), 7.44-7.37 (t, 1H, H-6, J = 9 Hz), 4.14-3.93 (m, 3H, NCH_2 & CH_{pyrr}), 2.84-2.66 (m, 2H, $COCH_2$); ESI-MS (m/z):

257.07 (M^+), 259.07 ($M^+ + H$); Anal. calcd. For $C_{11}H_9ClFNO_3$: C, 51.28; H, 3.52; N, 5.44. Found: C, 51.33; H, 3.57; N, 5.51.

4.1.1.6. 1-(4-Hydroxyphenyl)-5oxopyrrolidine-3-carboxylic acids (6)

White solid; Yield: 75 %; M.P.: 200-201 ºC; IR (KBr, cm^{-1}): 3267 (COO-H), 3064 (Ar C-H), 1751 (C=O), 1713 (C=OOH), 1537 (C=C); ^{1}H NMR (DMSO-d_6, 300 MHz) δ (ppm): 11.61 (s, 1H, COOH, D_2O exchangeable), 7.35-7.30 (d, 2H, H-2 & H-6, J = 7.5 Hz), 7.07-7.04 (d, 2H, H-3 & H-5, J = 9 Hz), 5.43 (s, 1H, OH), 4.11-3.92 (m, 3H, NCH_2 & CH_{pyrr}), 2.80-2.62 (m, 2H, $COCH_2$); ESI-MS (m/z): 221.11 (M^+); Anal. calcd. For $C_{11}H_{11}NO_4$: C, 59.73; H, 5.01; N, 6.33. Found: C, 59.82; H, 5.08; N, 6.41.

4.1.1.7. 1-(4-Methoxyphenyl)-5oxopyrrolidine-3-carboxylic acids (7)

White solid; Yield: 85 %; M.P.: 173-174 ºC; IR (KBr, cm^{-1}): 3254 (COO-H), 3051 (Ar C-H), 1739 (C=O), 1710 (C=OOH), 1571 (C=C); ^{1}H NMR (DMSO-d_6, 300 MHz) δ (ppm): 11.73 (s, 1H, COOH, D_2O exchangeable), 7.53-7.50 (d, 2H, H-2 & H-6, J = 9 Hz), 6.94-6.91 (d, 2H, H-3 & H-5, J = 9 Hz), 4.04-3.89 (m, 3H, NCH_2 & CH_{pyrr}), 2.80-2.61 (m, 2H, $COCH_2$); ESI-MS (m/z): 235.13 (M^+); Anal. calcd. For $C_{12}H_{13}NO_4$: C, 61.27; H, 5.57; N, 5.95. Found: C, 61.30; H, 5.63; N, 6.02.

4.1.1.8. 1-(4-Nitrophenyl)-5oxopyrrolidine-3-carboxylic acids (8)

Pale yellow solid; Yield: 33 %; M.P.: 175-177 ºC; IR (KBr, cm^{-1}): 3296 (COO-H), 3067 (Ar C-H), 1758 (C=O), 1722 (C=OOH), 1605 (C=C); ^{1}H NMR (DMSO-d_6, 300 MHz) δ (ppm): 11.64 (s, 1H, COOH, D_2O exchangeable), 7.92-7.87 (d, 2H, H-3 & H-5, J = 7.5 Hz), 7.06-7.01 (d, 2H, H-2 & H-6, J = 7.2 Hz), 4.13-3.95 (m, 3H, NCH_2 & CH_{pyrr}), 2.84-2.67 (m, 2H, $COCH_2$); ESI-MS (m/z): 250.11 (M^+); Anal. calcd. For $C_{11}H_{10}N_2O_5$: C, 52.80; H, 4.03; N, 11.20. Found: C, 52.91; H, 4.07; N, 11.31.

4.1.1.9. 1-(4-Sulfamoylphenyl)-5oxopyrrolidine-3-carboxylic acids (9)

White solid; Yield: 72 %; M.P.: 211-213 ºC; IR (KBr, cm^{-1}): 3278 (COO-H), 3068 (Ar C-H), 1760 (C=O), 1716 (C=OOH), 1591 (C=C); ^{1}H NMR (DMSO-d_6, 300 MHz) δ (ppm): 11.65 (s, 1H, COOH, D_2O exchangeable), 7.86-7.83 (d, 2H, H-3 & H-5, J = 9.3 Hz), 7.28-7.25 (d, 2H, H-2 & H-6, J = 8.1 Hz), 4.19-3.99 (m, 3H, NCH_2 & CH_{pyrr}), 3.56 (s, 2H, NH_2), 2.85-2.70 (m, 2H, $COCH_2$); ESI-MS (m/z): 284.10 (M^+); Anal. calcd. For $C_{11}H_{12}N_2O_5S$: C, 46.47; H, 4.25; N, 9.85. Found: C, 46.62; H, 4.37; N, 9.95.

*4.1.2. General procedure for the synthesis of 4-(benzothiazolyl/benzimidazolyl)-1-(substitutedphenyl)pyrrolidin-2-one derivatives (**10-27**)*

To an equimolar amount of appropriate 1-(substitutedphenyl)-5-oxopyrrolidine-3-carboxylic acids (10 mmol) and 2-aminobenzenethiol (10 mmol, 1.25 g) or 1,2-diaminobenzene (10 mmol, 1.08 g) in a round bottom flask, polyphosphoric acid (10 g) was added. The reaction mixture was stirred at 150-160 ^{o}C for 2-3 hours. The reaction mixture was then cooled to room temperature, 5% sodium carbonate solution (15 ml) was added, refluxed for 10 min and left to cool. The content of the flask was poured in a beaker containing 50 ml of water and stirred for 10 minutes. The crude product was filtered, washed with water and recrystallized from ethanol. The compounds were further purified through column chromatography by hexane:ethylacetate (4:1) as eluent.

4.1.2.1. 4-(Benzo[d]thiazol-2-yl)-1-phenylpyrrolidin-2-one (10)

Pale yellow solid; Yield: 60 %; M.P.: 148-149 ºC; IR (KBr, cm^{-1}): 3062 (Ar C-H), 1691 (C=O), 1606 (C=N), 1575 (C=C); ^{1}H NMR (DMSO-d_6, 300 MHz) δ (ppm): 8.17-7.15 (m, 9H, Ar-H), 4.39-4.17 (m, 3H, NCH_2 & CH_{pyrr}), 3.19-2.87 (m, 2H, $COCH_2$); ESI-MS (m/z): 294.10 (M^+), 295.10 (M^++H); Anal. calcd. For $C_{17}H_{14}N_2OS$: C, 69.36; H, 4.79; N, 9.52. Found: C, 69.43; H, 4.82; N, 9.61.

4.1.2.2. 4-(Benzo[d]thiazol-2-yl)-1-(2-methylphenyl)pyrrolidin-2-one (11)

Pale yellow solid; Yield: 63 %; M.P.: 155-156 ºC; IR (KBr, cm^{-1}): 3069 (Ar C-H), 1661 (C=O), 1597 (C=N), 1567 (C=C); ^{1}H NMR (DMSO-d_6, 300 MHz) δ (ppm): 8.11-8.08 (d, 1H, H-$4_{benzothiazole}$, J = 7.8 Hz), 8.00-7.97 (d, 1H, H-$7_{benzothiazole}$, J = 8.1 Hz), 7.53-7.35 (m, 4H, H-$5_{benzothiazole}$, H-$6_{benzothiazole}$, H-3_{phenyl} & H-4_{phenyl}), 7.20-7.17 (m, 2H, H-5_{phenyl} & H-6_{phenyl}), 4.38-4.25 (m, 2H, NCH_2), 4.17-4.12 (m, 1H, CH_{pyrr}), 3.18-2.88 (m, 2H, $COCH_2$), 2.17 (s, 3H, CH_3); ESI-MS (m/z): 308.13 (M^+), 309.13 (M^++H); Anal. calcd. For $C_{18}H_{16}N_2OS$: C, 70.10; H, 5.23; N, 9.08. Found: C, 70.27; H, 5.31; N, 9.17.

4.1.2.3. 4-(Benzo[d]thiazol-2-yl)-1-(4-methylphenyl)pyrrolidin-2-one (12)

Pale yellow solid; Yield: 65 %; M.P.: 152-153 ºC; IR (KBr, cm^{-1}): 3071 (Ar C-H), 1657 (C=O), 1591 (C=N), 1560 (C=C); ^{1}H NMR (DMSO-d_6, 300 MHz) δ (ppm): 8.11-8.08 (d, 1H, H-$4_{benzothiazole}$, J = 7.8 Hz), 8.00-7.97 (d, 1H, H-$7_{benzothiazole}$, J = 8.1 Hz), 7.57-7.41 (m, 4H, H-$5_{benzothiazole}$, H-$6_{benzothiazole}$, H-3_{phenyl} & H-5_{phenyl}), 7.20-7.17 (d, 2H, H-2_{phenyl} & H-6_{phenyl}, J = 8.4 Hz), 4.38-4.23 (m, 2H, NCH_2), 4.16-4.12 (m, 1H, CH_{pyrr}), 3.17-2.87 (m, 2H, $COCH_2$), 2.28 (s, 3H, CH_3); ESI-MS (m/z): 308.13 (M^+), 309.13 (M^++H); Anal. calcd. For $C_{18}H_{16}N_2OS$: C, 70.10; H, 5.23; N, 9.08. Found: C, 70.22; H, 5.33; N, 9.20.

4.1.2.4. 4-(Benzo[d]thiazol-2-yl)-1-(4-chlorophenyl)pyrrolidin-2-one (13)

Pale yellow solid; Yield: 63 %; M.P.: 174-175 ºC; IR (KBr, cm^{-1}): 3066 (Ar C-H), 1689 (C=O), 1610 (C=N), 1581 (C=C), 762 (C-Cl); ^{1}H NMR (DMSO-d_6, 300 MHz) δ (ppm): 8.10-8.08 (d, 1H, H-$4_{benzothiazole}$, *J* = 7.8 Hz), 7.99-7.97 (d, 1H, H-$7_{benzothiazole}$, *J* = 7.8 Hz), 7.74-7.71 (t, 2H, H-$5_{benzothiazole}$ & H-$6_{benzothiazole}$, J = 8.7 Hz), 7.59-7.42 (m, 4H, Ar-H_{phenyl}), 4.40-4.22 (m, 2H, NCH_2), 4.19-4.14 (m, 1H, CH_{pyrr}), 3.19-2.87 (m, 2H, $COCH_2$); ESI-MS (m/z): 328.08 (M^+), 330.08 (M^++2); Anal. calcd. For $C_{17}H_{13}ClN_2OS$: C, 62.10; H, 3.98; N, 8.52. Found: C, 62.21; H, 4.05; N, 8.63.

4.1.2.5. 4-(Benzo[d]thiazol-2-yl)-1-(3-chloro-4-fluorophenyl)pyrrolidin-2-one (14)

Pale yellow solid; Yield: 66 %; M.P.: 195-196 ºC; IR (KBr, cm^{-1}): 3112 (Ar C-H), 1680 (C=O), 1602 (C=N), 1535 (C=C), 771 (C-Cl); ^{1}H NMR (DMSO-d_6, 300 MHz) δ (ppm): 8.12-8.10 (d, 1H, H-$4_{benzothiazole}$, *J* = 7.8 Hz), 8.01-7.99 (d, 1H, H-$7_{benzothiazole}$, *J* = 7.8 Hz), 7.59-7.42 (m, 5H, Ar-H), 4.40-4.26 (m, 2H, NCH_2), 4.20-4.14 (m, 1H, CH_{pyrr}), 3.17-2.92 (m, 2H, $COCH_2$); ESI-MS (m/z): 346.05 (M^+), 348.05 (M^++2); Anal. calcd. For $C_{17}H_{12}ClFN_2OS$: C, 58.88; H, 3.49; N, 8.08. Found: C, 58.97; H, 3.55; N, 8.21.

4.1.2.6. 4-(Benzo[d]thiazol-2-yl)-1-(4-hydroxyphenyl)pyrrolidin-2-one (15)

Pale yellow solid; Yield: 52 %; M.P.: 169-170 ºC; IR (KBr, cm^{-1}): 3433 (O-H), 3096 (Ar C-H), 1680 (C=O), 1593 (C=N), 1525 (C=C); ^{1}H NMR (DMSO-d_6, 300 MHz) δ (ppm): 8.11-8.09 (d, 1H, H-$4_{benzothiazole}$, *J* = 7.8 Hz), 7.97-7.95 (d, 1H, H-$7_{benzothiazole}$, *J* = 7.8 Hz), 7.70-7.67 (t, 2H, H-$5_{benzothiazole}$ & H-$6_{benzothiazole}$, *J* = 8.7 Hz), 7.40-7.31 (m, 4H, Ar-H_{phenyl}), 5.65 (bs, 1H, OH, D_2O exchangeable), 4.38-4.23 (m, 2H, NCH_2), 4.15-4.11 (m, 1H, CH_{pyrr}), 3.17-2.91 (m, 2H, $COCH_2$); ESI-MS (m/z): 310.10 (M^+), 311.10 (M^++H); Anal. calcd. For $C_{17}H_{14}N_2O_2S$: C, 65.79; H, 4.55; N, 9.03. Found: C, 65.91; H, 4.67; N, 9.18.

4.1.2.7. 4-(Benzo[d]thiazol-2-yl)-1-(4-methoxyphenyl)pyrrolidin-2-one (16)

Pale yellow solid; Yield: 58 %; M.P.: 164-165 ºC; IR (KBr, cm^{-1}): 3091 (Ar C-H), 1685 (C=O), 1600 (C=N), 1547 (C=C); ^{1}H NMR (DMSO-d_6, 300 MHz) δ (ppm): 8.12-8.09 (d, 1H, H-$4_{benzothiazole}$, *J* = 7.8 Hz), 8.01-7.98 (d, 1H, H-$7_{benzothiazole}$, *J* = 8.1 Hz), 7.59-7.42 (m, 4H, H-$5_{benzothiazole}$, H-$6_{benzothiazole}$, H-3_{phenyl} & H-5_{phenyl}), 7.18-7.15 (d, 2H, H-2_{phenyl} & H-6_{phenyl}, *J* = 8.4 Hz), 4.40-4.22 (m, 2H, NCH_2), 4.15-4.09 (m, 1H, CH_{pyrr}), 3.69 (s, 3H, OCH_3), 3.15-2.86 (m, 2H, $COCH_2$); ESI-MS (m/z): 324.12 (M^+), 325.12 (M^++H); Anal. calcd. For $C_{18}H_{16}N_2O_2S$: C, 66.65; H, 4.97; N, 8.64. Found: C, 66.74; H, 5.08; N, 8.78.

4.1.2.8. 4-(Benzo[d]thiazol-2-yl)-1-(4-nitrophenyl)pyrrolidin-2-one (17)

Yellow solid; Yield: 55 %; M.P.: 209-210 ºC; IR (KBr, cm^{-1}): 3082 (Ar C-H), 1665 (C=O), 1598 (C=N), 1537 (C=C); ^{1}H NMR (DMSO-d_6, 300 MHz) δ (ppm): 8.28-8.11 (m, 4H, H-$4_{benzothiazole}$, H-$7_{benzothiazole}$, H-3_{phenyl} & H-5_{phenyl}), 7.52-7.38 (t, 2H, H-$5_{benzothiazole}$, H-$6_{benzothiazole}$, J = 8.7 Hz), 7.02-6.99 (d, 2H, H-2_{phenyl} & H-6_{phenyl}, J = 8.4 Hz), 4.37-4.18 (m, 2H, NCH_2), 4.13-4.10 (m, 1H, CH_{pyrr}), 3.12-2.85 (m, 2H, $COCH_2$); ESI-MS (m/z): 339.10 (M^+), 340.10 (M^++H); Anal. calcd. For $C_{17}H_{13}N_3O_3S$: C, 60.17; H, 3.86; N, 12.38. Found: C, 60.25; H, 3.97; N, 12.51.

4.1.2.9. 4-(Benzo[d]thiazol-2-yl)-1-(4-sulfamoylphenyl)pyrrolidin-2-one (18)

Pale yellow solid; Yield: 52 %; M.P.: 188-189 ºC; IR (KBr, cm^{-1}): 3093 (Ar C-H), 1674 (C=O), 1604 (C=N), 1534 (C=C); ^{1}H NMR (DMSO-d_6, 300 MHz) δ (ppm): 8.17-8.05 (m, 4H, Ar-H), 7.55-7.42 (m, 4H, Ar-H), 5.71 (s, 2H, SO_2NH_2, D_2O exchangeable) 4.37-4.22 (m, 2H, NCH_2), 4.19-4.14 (m, 1H, CH_{pyrr}), 3.19-2.87 (m, 2H, $COCH_2$); ESI-MS (m/z): 373.09 (M^+), 374.09 (M^++H); Anal. calcd. For $C_{17}H_{15}N_3O_3S_2$: C, 54.68; H, 4.05; N, 11.25. Found: C, 54.82; H, 4.16; N, 11.31.

4.1.2.10. 4-(1H-benzo[d]imidazol-2-yl)-1-phenylpyrrolidin-2-one (19)

Off white solid; Yield: 75 %; M.P.: 215-216 ºC; IR (KBr, cm^{-1}): 3387 (N-H), 3161 (Ar C-H), 1695 (C=O), 1592 (C=N), 1568 (C=C); ^{1}H NMR (DMSO-d_6, 300 MHz) δ (ppm): 12.48 (bs, 1H, NH, D_2O exchangeable), 7.69-7.67 (d, 2H, H-$4_{benzimidazole}$ and H-$7_{benzimidazole}$, J = 8.1 Hz), 7.52-7.36 (m, 4H, ArH), 7.17-7.12 (m, 3H, ArH), 4.32-4.19 (m, 2H, NCH_2), 4.05-3.95 (m, 1H, CH_{pyrr}), 3.10-2.93 (m, 2H, $COCH_2$); ESI-MS (m/z): 277.15 (M^+), 278.15 (M^++H); Anal. calcd. For $C_{17}H_{15}N_3O$: C, 73.63; H, 5.45; N, 15.15. Found: C, 73.70; H, 5.51; N, 15.22.

4.1.2.11. 4-(1H-benzo[d]imidazol-2-yl)-1-(2-methylphenyl)pyrrolidin-2-one (20)

Off white solid; Yield: 72 %; M.P.: 220-221 ºC; IR (KBr, cm^{-1}): 3415 (N-H), 3189 (Ar C-H), 1695 (C=O), 1605 (C=N), 1576 (C=C); ^{1}H NMR (DMSO-d_6, 300 MHz) δ (ppm): 12.45 (bs, 1H, NH, D_2O exchangeable), 7.69-7.51 (m, 4H, ArH), 7.47-7.31 (m, 4H, ArH), 4.32-4.20 (m, 2H, NCH_2), 4.07-3.97 (m, 1H, CH_{pyrr}), 3.10-2.89 (m, 2H, $COCH_2$), 2.22 (s, 3H, CH_3); ESI-MS (m/z): 291.17 (M^+), 292.17 (M^++H); Anal. calcd. For $C_{18}H_{17}N_3O$: C, 74.20; H, 5.88; N, 14.42. Found: C, 74.32; H, 5.96; N, 14.55.

4.1.2.12. 4-(1H-benzo[d]imidazol-2-yl)-1-(4-methylphenyl)pyrrolidin-2-one (21)

Off white solid; Yield: 75 %; M.P.: 218-219 ºC; IR (KBr, cm^{-1}): 3395 (N-H), 3177 (Ar C-H), 1670 (C=O), 1587 (C=N), 1572 (C=C); ^{1}H NMR (DMSO-d_6, 300 MHz) δ (ppm): 12.19 (bs, 1H, NH, D_2O exchangeable), 7.57-7.51 (m, 4H, ArH), 7.20-7.15 (m, 4H, ArH), 4.29-4.16 (m, 2H, NCH_2), 4.06-3.95 (m, 1H, CH_{pyrr}), 3.08-2.92 (m, 2H, $COCH_2$), 2.28 (s, 3H, CH_3); ESI-MS (m/z): 291.17

(M^+), 292.17 (M^++H); Anal. calcd. For $C_{18}H_{17}N_3O$: C, 74.20; H, 5.88; N, 14.42. Found: C, 74.35; H, 5.95; N, 14.57.

4.1.2.13. 4-(1H-benzo[d]imidazol-2-yl)-1-(4-chlorophenyl)pyrrolidin-2-one (22)

Off white solid; Yield: 72 %; M.P.: 212-213 ºC; IR (KBr, cm^{-1}): 3405 (N-H), 3117 (Ar C-H), 1683 (C=O), 1588 (C=N), 1552 (C=C); ^{1}H NMR (DMSO-d_6, 300 MHz) δ (ppm): 12.38 (bs, 1H, NH, D_2O exchangeable), 7.72-7.69 (d, 2H, H-$4_{benzimidazole}$ and H-$7_{benzimidazole}$, J = 9 Hz), 7.52-7.34 (m, 4H, ArH), 7.16-7.13 (m, 2H, ArH), 4.30-4.16 (m, 2H, NCH_2), 4.05-3.95 (m, 1H, CH_{pyrr}), 3.09-2.93 (m, 2H, $COCH_2$); ESI-MS (m/z): 311.12 (M^+), 313.12 (M^++2); Anal. calcd. For $C_{17}H_{14}ClN_3O$: C, 65.49; H, 4.53; N, 13.48. Found: C, 65.58; H, 4.65; N, 13.56.

4.1.2.14. 4-(1H-benzo[d]imidazol-2-yl)-1-(3-chloro-4-fluorophenyl)pyrrolidin-2-one (23)

Off white solid; Yield: 74 %; M.P.: 253-254 ºC; IR (KBr, cm^{-1}): 3380 (N-H), 3121 (Ar C-H), 1678 (C=O), 1590 (C=N), 1542 (C=C); ^{1}H NMR (DMSO-d_6, 300 MHz) δ (ppm): 12.49 (bs, 1H, NH, D_2O exchangeable), 8.01-7.98 (m, 1H, ArH), 7.66-7.41 (m, 4H, ArH), 7.17-7.14 (m, 2H, ArH), 4.32-4.19 (m, 2H, NCH_2), 4.05-3.95 (m, 1H, CH_{pyrr}), 3.11-2.94 (m, 2H, $COCH_2$); ESI-MS (m/z): 329.10 (M^+), 331.10 (M^++2); Anal. calcd. For $C_{17}H_{13}ClFN_3O$: C, 61.92; H, 3.97; N, 12.74. Found: C, 62.18; H, 4.09; N, 12.85.

4.1.2.15. 4-(1H-benzo[d]imidazol-2-yl)-1-(4-hydroxyphenyl)pyrrolidin-2-one (24)

Off white solid; Yield: 68 %; M.P.: 228-229 ºC; IR (KBr, cm^{-1}): 3421(O-H), 3106 (Ar C-H), 1679 (C=O), 1595 (C=N), 1525 (C=C); ^{1}H NMR (DMSO-d_6, 300 MHz) δ (ppm): 12.37 (bs, 1H, NH, D_2O exchangeable), 7.73-7.58 (m, 4H, ArH), 7.44-7.15 (m, 4H, ArH), 5.63 (bs, 1H, OH, D_2O exchangeable), 4.33-4.20 (m, 2H, NCH_2), 4.06-3.97 (m, 1H, CH_{pyrr}), 3.10-2.89 (m, 2H, $COCH_2$); ESI-MS (m/z): 293.14 (M^+), 294.14 (M^++H); Anal. calcd. For $C_{17}H_{15}N_3O_2$: C, 69.61; H, 5.15; N, 14.33. Found: C, 69.80; H, 5.22; N, 14.49.

4.1.2.16. 4-(1H-benzo[d]imidazol-2-yl)-1-(4-methoxyphenyl)pyrrolidin-2-one (25)

Off white solid; Yield: 70 %; M.P.: 224-225 ºC; IR (KBr, cm^{-1}): 3380 (N-H), 3172 (Ar C-H), 1692 (C=O), 1603 (C=N), 1575 (C=C); ^{1}H NMR (DMSO-d_6, 300 MHz) δ (ppm): 12.40 (bs, 1H, NH, D_2O exchangeable), 7.77-7.54 (m, 4H, ArH), 7.43-7.13 (m, 4H, ArH), 4.31-4.17 (m, 2H, NCH_2), 4.07-3.98 (m, 1H, CH_{pyrr}), 3.72 (s, 3H, OCH_3), 3.08-2.92 (m, 2H, $COCH_2$); ESI-MS (m/z): 307.16 (M^+), 308.17 (M^++H); Anal. calcd. For $C_{18}H_{17}N_3O_2$: C, 70.34; H, 5.58; N, 13.67. Found: C, 70.42; H, 5.65; N, 13.74.

4.1.2.17. 4-(1H-benzo[d]imidazol-2-yl)-1-(4-nitrophenyl)pyrrolidin-2-one (26)

Yellow solid; Yield: 60 %; M.P.: 271-272 ºC; IR (KBr, cm^{-1}): 3120 (Ar C-H), 1670 (C=O), 1587 (C=N), 1531 (C=C); ^{1}H NMR (DMSO-d_6, 300 MHz) δ (ppm): 12.35 (bs, 1H, NH, D_2O exchangeable), 7.81-7.55 (m, 4H, Ar-H), 7.41-7.13 (m, 4H, ArH), 4.31-4.17 (m, 2H, NCH_2), 4.06-3.96 (m, 1H, CH_{pyrr}), 3.10-2.93 (m, 2H, $COCH_2$); ESI-MS (m/z): 322.13 (M^+), 323.13 (M^++H); Anal. calcd. For $C_{17}H_{14}N_4O_3$: C, 63.35; H, 4.38; N, 17.38. Found: C, 63.47; H, 4.55; N, 17.51.

4.1.2.18. 4-(1H-benzo[d]imidazol-2-yl)-1-(4-sulfamoylphenyl)pyrrolidin-2-one (27)

Pale yellow solid; Yield: 62 %; M.P.: 233-234 ºC; IR (KBr, cm^{-1}): 3122 (Ar C-H), 1690 (C=O), 1598 (C=N), 1541 (C=C); ^{1}H NMR (DMSO-d_6, 300 MHz) δ (ppm): 12.41 (bs, 1H, NH, D_2O exchangeable), 7.61-7.49 (m, 4H, Ar-H), 7.34-7.19 (m, 4H, ArH), 5.78 (s, 2H, SO_2NH_2, D_2O exchangeable), 4.37-4.22 (m, 2H, NCH_2), 4.19-3.14 (m, 1H, CH_{pyrr}), 3.19-2.87 (m, 2H, $COCH_2$); ESI-MS (m/z): 356.10 (M^+), 357.11 (M^++H); Anal. calcd. For $C_{17}H_{16}N_4O_3S$: C, 57.29; H, 4.53; N, 15.72. Found: C, 57.38; H, 4.64; N, 15.88.

4.2. In vitro hMAGL enzyme inhibition assay

The hMAGL enzyme inhibition assay was done by the method reported previously and as per the manufacturer's instructions supplied with Cayman's assay kit, USA [33,36]. In short, six concentration of test compounds (10-27) and standard (CAY10499) in DMSO as solvent, ranging 100 µM to 1 nM, were prepared by serial dilution (tenfold) method. The samples were tested for their potential to inhibit MAGL in triplicate, using 180 µl, in 96-well plates, as provided with the assay kit. Tris-HCl (10 mM, pH 7.2), containing EDTA (1mM) and BSA (0.1 mg/ml) was used as assay buffer and for the dilution of *h*MAGL protein. 4-nitrophenylacetate (4-NPA) was used as MAGL substrate, which gives yellow coloured product (4-nitrophenol) upon MAGL action. Average absorbance of background well containing DMSO and buffer (BW), 100% initial activity wells (IA), test samples and standard sample were recorded at 405 nm using microplate reader (PerkinElmer®). The average absorbance of BW was then subtracted from the average absorbance of IA, test samples and standard samples. The percentage MAGL activity for the test and standard samples were determined by the formula: % MAGL activity = Test / IA × 100. GraphPad Prism (ver. 6.01) was used for the calculation of IC_{50} values (**Table 1**).

4.3. In vitro hFAAH enzyme inhibition assay

The *h*FAAH enzyme inhibition assay was done by the method reported previously and as per the manufacturer's instructions supplied with Cayman's assay kit, USA [37]. Six concentrations of test compounds (**22**, **23** and **25**) and standard (URB597) in DMSO as solvent, ranging 100 µM to 1 nM, were prepared by serial dilution (tenfold) method. The samples were tested for their potential

to inhibit FAAH in triplicate, using 180 µl, in 96-well plates, as provided with the assay kit. Tris-HCl (125 mM, pH 9), containing EDTA (1mM) and BSA (0.1 mg/ml) was used as assay buffer and for the dilution of *h*FAAH protein. AMC arachidonoylamide (AMCAA) was used as FAAH substrate. Average fluorescence of BW (background well containing DMSO and buffer), 100% initial activity wells (IA), test samples and standard sample were recorded at 340 nm (excitation wavelength) and 460 nm (emission wavelength) using microplate reader (PerkinElmer®). The average fluorescence of BW was then subtracted from the average absorbance of IA, test samples and standard samples. The percentage FAAH activity for the test and standard samples were determined by the formula: % FAAH activity = Test / IA × 100. GraphPad Prism (ver. 6.01) was used for the calculation of IC_{50} values (**Table 1**).

4.4. Computational study

Computations were performed on an Intel Core i7, 4.90 GHz processor with 16 GB memory and 2 GB graphics running with Windows 10 operating system. Maestro10.1 graphical user interface (GUI) of Schrödinger was utilized for computations.

4.4.1. Molecular docking

Glide 5.9 implemented in Maestro 9.4 (GUI of Schrodinger) was used for extra precision (XP) docking of potential ligand (compound 25). The X-ray crystal structure of *h*MAGL (PDB ID: 5ZUN, Resolution-1.35 Å) was retrieved from Protein Data Bank (PDB) and utilized for molecular docking study [29]. Protein Preparation Wizard in Maestro was used for the protein structure preparation like deletion of water molecules, assignment of bond orders, the inclusion of hydrogen atoms, and treatment of formal charges. An exhaustive sampling option was utilized for the optimization of the hydrogen bonding network. The energy of the protein structure was minimized to an RMSD of 0.3 Å by using the Impref module (Impact 5.9) with the OPLS_2005 force field. Glide scoring grids (docking grid box of 20×20×20 Å) were generated by defining the active binding site residues in the protein structure. LigPrep 2.6 with Epik 2.4, were used to expand protonation, and tautomeric states of ligand (compound 25) at pH 7.0 ± 2.0 and then energy was minimized using the OPLS_2005 force field. The docking simulation of the prepared ligand was performed by Glide XP docking [39].

4.4.2. Physicochemical and pharmacokinetic properties

The QikProp 3.6 of Schrodinger is used for the calculation of physicochemical and pharmacokinetic properties of the selected compounds (compound 22, 23 and 25). Structures of the compounds were neutralised prior to the generation of QikProp (QP) properties. Thirty-five

physicochemical and pharmacokinetic properties were predicted and compared with the qualifying limits as proposed for orally active CNS drug discovery [40].

4.5. Antinociceptive activity

Animals were obtained from Central Animal House Facility, Jamia Hamdard (Hamdard University), New Delhi-110062 (Registration Number: 173/CPCSEA; 28 Jan., 2000). All the experimental procedures were carried out with the permission of Institutional Animal Ethics Committee (Proposal No. 1048). The rats were housed under standard laboratory conditions (Temperature: 22±3ºC; RH: 60±5% and 12/12 hours light-dark cycle) in polypropylene cages. Animals were provided free access to standard diet pellets (Amrut rat feed, Mfd. by Nav Maharastra Chakan Oil Mills Ltd., New Delhi, India) and water *ad libitum*. The animals were selected randomly, marked and housed in their cages for 7 days prior to dosing to allow for acclimatisation to the laboratory conditions.

4.5.1. Formalin-induced nociception test

Formalin test was performed by the method reported in literature [41,42]. Male Wistar rats (180-200 g, at the time of dosing) were taken in groups of ten animals each. Animals were administered vehicle (0.5% methylcellulose) or test compound 25 (5, 10, 30 and 50 mg/kg; p.o; suspended in 0.5% methylcellulose), 4 hours before an intraplantar injection of formalin (2.5%, 50 µl) into the dorsal surface of the right hind paw. The reference drug, GBP (100 mg/kg, i.p, dissolved in 0.9% normal saline), was injected 30 minutes before formalin injection. The duration of time (in seconds) spent licking and biting the injected paw, was recorded in the time interval of 0-5 minutes (phase-I, acute chemical pain consist of intense licking and biting) and 10-30 minutes (phase-II, state of central sensitization, which involves periods of licking and biting), after formalin injection.

4.6. Statistical analysis

GraphPad Prism (ver. 6.01) was used for statistical analysis of data. Treatment effects were compared with the control by using analysis of variance (ANOVA) followed by Dunnett's test. Results are expressed as mean±SEM.

Conflict of Interest

The authors have declared no conflict of interest.

Acknowledgments

The authors would like to thank the Deanship of Scientific Research at Prince Sattam Bin Abdulaziz University for providing financial support for this project (grant no. 2019/03/11064).

Data Availability Statement

The data that support the findings of this study are available on request from the corresponding author.

References

1. Karlsson, M., Contreras, J., Hellman, U., Tornqvist, H., Holm, C. (1997). cDNA cloning, tissue distribution, and identification of the catalytic triad of monoglyceride lipase. Evolutionary relationship to esterases, lysophospholipases, and haloperoxidases. J. Biol. Chem. 272, 27218-27223.
2. Chon, S.H., Zhou, Y.X., Dixon, J.L., Storch, J. (2007). Intestinal monoacylglycerol metabolism: developmental and nutritional regulation of monoacylglycerol lipase and monoacylglycerol acyltransferase, J. Biol. Chem. 282, 33346–33357.
3. Ueda, N., Tsuboi, K., Uyama, T., Ohnishi, T. (2011). Biosynthesis and degradation of the endocannabinoid 2-arachidonoylglycerol, Biofactors. 37, 1-7.
4. Lass, A., Zimmermann, R., Oberer, M., Zechner, R. (2011). Lipolysis – a highly regulated multi-enzyme complex mediates the catabolism of cellular fat stores, Prog. Lipid Res. 50, 14-27.
5. DiMarzo, V., DePetrocellis, L., Bisogno, T. (2005). The biosynthesis, fate and pharmacological properties of endocannabinoids. Handb. Exp. Pharmacol. 168, 147-185.
6. Blankman, J.L., Simon, G.M., Cravatt, B.F. (2007). A comprehensive profile of brain enzymes that hydrolyze the endocannabinoid 2-arachidonoylglycerol. Chem. Biol. 14, 1347-1356.
7. Savinainen, J.R., Saario, S.M., Laitinen, J.T. (2012). The serine hydrolases MAGL, ABHD6 and ABHD12 as guardians of 2-arachidonoylglycerol signalling through cannabinoid receptors. Acta Physiol. (Oxf.) 204, 267-276.
8. Nomura, D.K., Morrison, B.E., Blankman, J.L., Long, J.Z., Kinsey, S.G., Marcondes, M.C., Ward, A.M., Hahn, Y.K., Lichtman, A.H., Conti, B., Cravatt, B.F. (2011). Endocannabinoid hydrolysis generates brain prostaglandins that promote neuroinflammation. Science. 334, 809-813.

9. Chen, R., Zhang, J., Wu, Y., Wang, D., Feng, G., Tang, Y.P., Teng, Z., Chen, C. (2012). Monoacylglycerol lipase is a therapeutic target for Alzheimer's disease. Cell Rep. 2, 1329-1339.
10. Kinsey, S.G., Long, J.Z., O'Neal, S.T., Abdullah, R.A., Poklis, J.L., Boger, D., Cravatt, B.F., Lichtman, A.H. (2009). Blockade of endocannabinoid-degrading enzymes attenuates neuropathic pain. J. Pharmacol. Exp. Ther. 330, 902-910.
11. Kinsey, S.G., Long, J.Z., Cravatt, B.F., Lichtman, A.H. (2010). Fatty acid amide hydrolase and monoacylglycerol lipase inhibitors produce anti-allodynic effects in mice through distinct cannabinoid receptor mechanisms. J. Pain. 11, 1420-1428.
12. Hohmann, A.G., Suplita, R.L., Bolton, N.M., Neely, M.H., Fegley, D., Mangieri, R., Krey, J.F., Walker, J.M., Holmes, P.V., Crystal, J.D., Duranti, A., Tontini, A., Mor, M., Tarzia, G., Piomelli, D. (2005). An endocannabinoid mechanism for stress-induced analgesia. Nature. 435, 1108-1112.
13. Connell, K., Bolton, N., Olsen, D., Piomelli, D., Hohmann, A.G. (2006). Role of the basolateral nucleus of the amygdala in endocannabinoid-mediated stress-induced analgesia. Neurosci. Lett. 397, 180-184.
14. Guindon, J., Guijarro, A., Piomelli, D., Hohmann, A.G. (2011). Peripheral antinociceptive effects of inhibitors of monoacylglycerol lipase in a rat model of inflammatory pain. Br. J. Pharmacol. 163, 1464-1478.
15. Guindon, J., Lai, Y., Takacs, S.M., Bradshaw, H.B., Hohmann, A.G. (2013). Alterations in endocannabinoid tone following chemotherapy-induced peripheral neuropathy: Effects of endocannabinoid deactivation inhibitors targeting fatty-acid amide hydrolase and monoacylglycerol lipase in comparison to reference analgesics following cisplatin treatment. Pharmacol. Res. 67, 94-109.
16. Aaltonen, N., Kedzierska, E., Orzelska-Górka, J., Lehtonen, M., Navia-Paldanius, D., Jakupovic, H., Savinainen, J.R., Nevalainen, T., Laitinen, J.T., Parkkari, T., Gynther, M. (2016). In Vivo Characterization of the Ultrapotent Monoacylglycerol Lipase Inhibitor {4-[bis-(benzo[d][1,3]dioxol-5-yl)methyl]-piperidin-1-yl}(1H-1,2,4-triazol-1-yl)methanone (JJKK-048). J. Pharm. Exp. Ther. 359, 62-72.
17. Fowler, C.J. (2012) Monoacylglycerol lipase - a target for drug development? Br. J. Pharmacol. 166, 1568-1585.

18. Mulvihill, M.M., Nomura, D.K. (2013) Therapeutic potential of monoacylglycerol lipase inhibitors. Life Sci. 92, 492-497.
19. Alhouayek, M., Masquelier, J., Muccioli, G.G. (2014). Controlling 2-arachidonoylglycerol metabolism as an anti-inflammatory strategy. Drug Discov. Today. 19, 295-304.
20. Bertrand, T., Auge, F., Houtmann, J., Rak, A., Vallee, F., Mikol, V., Berne, P.F., Michot, N., Cheuret, D., Hoornaert, C., Mathieu, M.J. (2010) Structural basis for human monoglyceride lipase inhibition. Mol. Biol. 396, 663-673.
21. Morera, L., Labar, G., Ortar, G., Lambert, D.M. (2010). Development and characterization of endocannabinoid hydrolases FAAH and MAGL inhibitors bearing a benzotriazol-1-yl carboxamide scaffold. Bioorg. Med. Chem. 20, 6260-6275.
22. Aaltonen, N., Savinainen, J.R., Ribas, C.R., Ronkko, J., Kuusisto, A., Korhonen, J., Paldanius, D.N., Hayrinen, J., Takabe, P., Kasnanen, H., Pantsar, T., Laitinen, T., Lehtonen, M., Seppanen, S.P., Poso, A., Nevalainen, T., Laitinen, J.T. (2013). Piperazine and piperidinetriazoleureas as ultrapotent and highly selective inhibitors of monoacylglycerol lipase. Chem. Biol. 20, 379-390.
23. Chang, J.W., Niphakis, M.J., Lum, K.M., Cognetta, A.B., Wang, C., Matthews, M.L., Niessen, S., Buczynski, M.W., Parsons, L.H., Cravatt, B.F. (2012). Remarkably selective inhibitors of monoacylglycerol lipase bearing a reactive group that is bioisosteric with endocannabinoid substrates. Chem. Biol. 19, 579-588.
24. Labar, G., Bauvois, C., Borel, F., Ferrer, J.L., Wouters, J., Lambert, D.M. (2010). Crystal structure of the human monoacylglycerol lipase, a key actor in endocannabinoid signaling. ChemBioChem. 11, 218-227.
25. Schalk-Hihi, C., Schubert, C., Alexander, R., Bayoumy, S., Clemente, J.C., Deckman, I., DesJarlais, R.L., Dzordzorme, K.C., Flores, C.M., Grasberger, B., Kranz, J.K., Lewandowski, F., Liu, L., Ma, H., Maguire, D., Macielag, M.J., McDonnell, M.E., Mezzasalma, H.T., Miller, R., Milligan, C., Reynolds, C., Kuo, L.C. (2011). Crystal structure of a soluble form of human monoglyceride lipase in complex with an inhibitor at 1.35 Å resolution. Protein Sci. 20, 670-683.
26. Scalvini, L., Piomelli, D., Mor, M. (2016). Monoglyceride lipase: Structure and inhibitors. Chem. Phys. Lipids. 197, 13-24.
27. Cisar, J.S., Weber, O.D., Clapper, J.R., Blankman, J.L., Henry, C.L., Simon, G.M., Alexander, J.P., Jones, T.K., Ezekowitz, R.A.B., O'Neill, G.P., Grice, C.A. (2018).

Identification of ABX-1431, a Selective Inhibitor of Monoacylglycerol Lipase and Clinical Candidate for Treatment of Neurological Disorders. J. Med. Chem. 61, 9062-9084.

28. McAllister, L.A., Butler, C.R., Mente, S., O'Neil, S.V., Fonseca, K.R., Piro, J.R., Cianfrogna, J.A., Foley, T.L., Gilbert, A.M., Harris, A.R., Helal, C.J., Johnson, D.S., Montgomery, J.I., Nason, D.M., Noell, S., Pandit, J., Rogers, B.N., Samad, T.A., Shaffer, C.L., DaSilva, R.G., Uccello, D.P., Webb, D., Brodney, M.A. (2018). Discovery of Trifluoromethyl Glycol Carbamates as Potent and Selective Covalent Monoacylglycerol Lipase (MAGL) Inhibitors for Treatment of Neuroinflammation. J. Med. Chem. 61, 3008-3026.
29. Aida, J., Fushimi, M., Kusumoto, T., Sugiyama, H., Arimura, N., Ikeda, S., Sasaki, M., Sogabe, S., Aoyama, K., Koike, T. (2018). Design, Synthesis, and Evaluation of Piperazinyl Pyrrolidin-2-ones as a Novel Series of Reversible Monoacylglycerol Lipase Inhibitors. J. Med. Chem. 61, 9205-9217.
30. Granchi, C., Lapillo, M., Glasmacher, S., Bononi, G., Licari, C., Poli, G., ElBoustani, M., Caligiuri, I., Rizzolio, F., Gertsch, J., Macchia, M., Minutolo, F., Tuccinardi, T., Chicca, A. (2019). Optimization of a Benzoylpiperidine Class Identifies a Highly Potent and Selective Reversible Monoacylglycerol Lipase (MAGL) Inhibitor. J. Med. Chem. 62, 1932-1958.
31. Castelli, R., Scalvini, L., Vacondio, F., Lodola, A., Anselmi, M., Vezzosi, S., Carmi, C., Bassi, M., Ferlenghi, F., Rivara, S., Møller, I.R., Rand, K.D., Daglian, J., Wei, D., Dotsey, E.Y., Ahmed, F., Jung, K.M., Stella, N., Singh, S., Mor, M., Piomelli, D. (2020). Benzisothiazolinone Derivatives as Potent Allosteric Monoacylglycerol Lipase Inhibitors That Functionally Mimic Sulfenylation of Regulatory Cysteines. J. Med. Chem. 63, 1261-1280.
32. Afzal, O., Kumar, S., Kumar, R., Firoz, A., Jaggi, M., Bawa, S. (2014). Docking based virtual screening and molecular dynamics study to identify potential monoacylglycerol lipase inhibitors. Bioorg. Med. Chem. Lett. 24, 3986-3996.
33. Afzal, O., Akhtar, M.S., Kumar, S., Ali, M.R., Jaggi, M., Bawa, S. (2016). Hit to lead optimization of a series of N-[4-(1,3-benzothiazol-2-yl)phenyl]acetamides as monoacylglycerol lipase inhibitors with potential anticancer activity. Eur. J. Med. Chem. 121, 318-330.

34. Paytash, P.L., Sparrow, E., Gathe, J.C. (1950) The reaction of itaconic acid with primary amines. J. Am. Chem. Soc. 72, 1415-1416.
35. Mickevicius, M., Beresnevicius, Z.J., Mickevicius, V., Mikulskiene, G. (2006). Condensation Products of 1-Aryl-4-carboxy-2- pyrrolidinones with o-Diaminoarenes, o-Aminophenol, and Their Structural Studies. Heteroatom Chem. 17, 47-56.
36. Muccioli, G., Labar, G., Lambert, D. (2008). CAY10499, a novel monoglyceride lipase inhibitor evidenced by an expeditious MGL assay, Chembiochem. 9, 2704-2710.
37. Granchi, C., Rizzolio, F., Palazzolo, S., Carmignani, S., Macchia, M., Saccomanni, G., Manera, C., Martinelli, A., Minutolo, F., Tuccinardi, T. (2016). Structural Optimization of 4-Chlorobenzoylpiperidine Derivatives for the Development of Potent, Reversible, and Selective Monoacylglycerol Lipase (MAGL) Inhibitors, J. Med. Chem. 59, 10299-10314.
38. Mor, M., Rivara, S., Lodola, A., Plazzi, P.V., Tarzia, G., Duranti, A., Tontini, A., Piersanti, G., Kathuria, S., Piomelli, D. (2004). Cyclohexylcarbamic Acid 3′- or 4′-Substituted Biphenyl-3-yl Esters as Fatty Acid Amide Hydrolase Inhibitors: Synthesis, Quantitative Structure-Activity Relationships, and Molecular Modeling Studies. J. Med. Chem. 47, 4998-5008.
39. Friesner, R.A., Murphy, R.B., Repasky, M.P., Frye, L.L., Greenwood, J.R., Halgren, T.A., Sanschagrin, P.C., Mainz, D.T. (2006). Extra precision glide: docking and scoring incorporating a model of hydrophobic enclosure for protein-ligand complexes. J. Med. Chem. 49, 6177-6196.
40. Ghose, A.K., Herbertz, T., Hudkins, R.L., Dorsey, B.D., Mallamo, J.P. (2012). Knowledge-Based, Central Nervous System (CNS) Lead Selection and Lead Optimization for CNS Drug Discovery. ACS Chem. Neurosci. 3, 50-68.
41. Coderre, T.J., Vaccarino, A.L., Melzack, R. (1990). Central nervous system plasticity in the tonic pain response to subcutaneous formalin injection. Brain Res. 535, 155-158.
42. Laughlin, T.M. Tram, K.V. Wilcox, G.L. Birnbaum, A.K. (2002). Comparison of antiepileptic drugs tiagabine, lamotrigine and gabapentin in mouse models of acute, prolonged and chronic nociception. J. Pharmacol. Exp. Ther. 302, 1168-1175.

Table 1: *In vitro h*MAGL and *h*FAAH inhibition assay of the synthesized compounds (**10-27**).

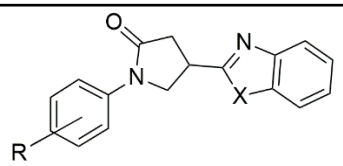

Compound	X	R	*h*MAGL IC_{50}	*h*FAAH IC_{50}
10	S	H	>100 μM	ND
11	S	2-CH_3	88 μM	ND
12	S	4-CH_3	>100 μM	ND

13	S	4-Cl	60 μM	ND
14	S	3-Cl,4-F	48 μM	ND
15	S	4-OH	>100 μM	ND
16	S	4-OCH_3	72 μM	ND
17	S	4-NO_2	>100 μM	ND
18	S	4-SO_2NH_2	>100 μM	ND
19	NH	H	680 nM	ND
20	NH	2-CH_3	255 nM	ND
21	NH	4-CH_3	290 nM	ND
22	NH	4-Cl	**8.6 nM**	35 μM
23	NH	3-Cl,4-F	**8.0 nM**	24 μM
24	NH	4-OH	22 μM	ND
25	NH	4-OCH_3	**9.4 nM**	52 μM
26	NH	4-NO_2	760 nM	ND
27	NH	4-SO_2NH_2	45 μM	ND
CAY10499	--	--	415 nM	--
URB597	--	--	--	5 nM

ND: Not Determined; CAY10499 and URB597 (standard control); IC_{50} values were calculated from GraphPad Prism (ver. 6.01).

Figure 1: MAGL substrate (2-AG) and representative potent MAGL inhibitors.

Figure 2: Design of novel MAGL inhibitors. (A) MAGL Substrate, 2-AG; (B) Binding pattern of MAGL inhibitors (ZINC12863377 AND ZINC24092691); (C) Designed compounds (10-27).

Figure 3: (Scheme 1): Synthesis of the intermediates (**1-9**) and target compounds (**10-27**).

Figure 4: 3D and 2D representation of MAGL-compound 25 binding pattern, obtained after glide XP docking.

Figure 5: Formalin induced nociception test; a single dose of the test compounds (5, 10, 30 and 50 mg/kg, p.o, suspended in 0.5% methylcellulose) was administered 4 hours before formalin injection (50 µl, 2.5%). Reference drug, gabapentin (100 mg/kg, i.p, dissolved in 0.9 % normal saline) was injected 30 minutes before formalin injection. Total paw licking and biting duration, Phase-I (white bar, 0-5 min.) and Phase-II (black bar, 10-30 min.) was recorded as a measure of pain behaviour. Data is represented as mean±SEM from a group of 10 animals. *$p<0.05$, **$p<0.01$, $p>0.05$ (NS, non-significant) vs. control (vehicle). GBP: gabapentin; T5, T10, T30, T50 are the dose concentration of tested compound-25.

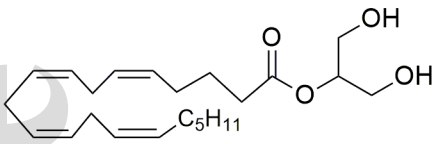

2-AG (1)

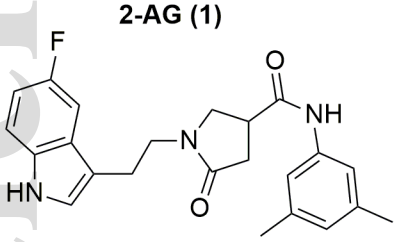

ZINC12863377
IC_{50} = 39 nM

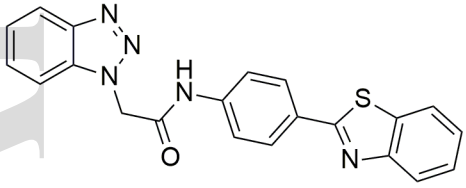

ZINC24092691
IC_{50} = 10 nM

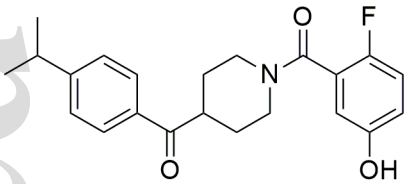

Compound 23
IC_{50} = 80 nM

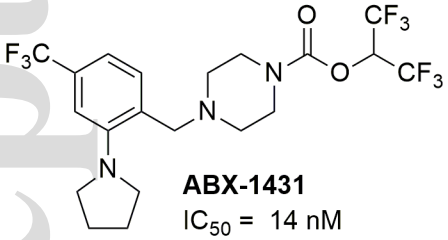

ABX-1431
IC_{50} = 14 nM

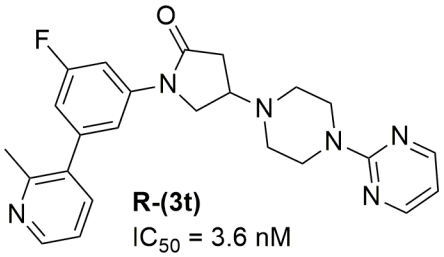

R-(3t)
IC_{50} = 3.6 nM

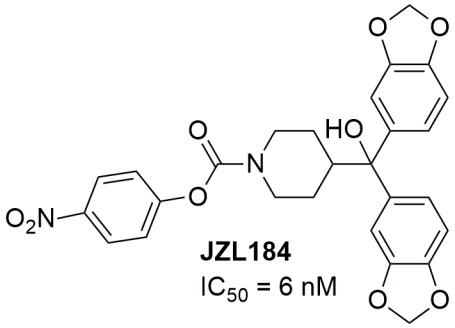

JZL184
IC_{50} = 6 nM

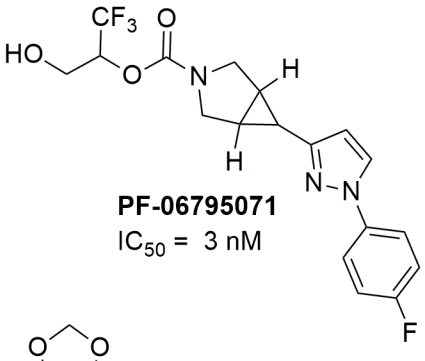

PF-06795071
IC_{50} = 3 nM

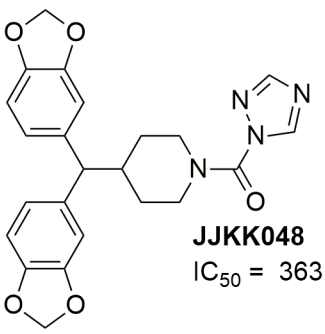

JJKK048
IC_{50} = 363 pM

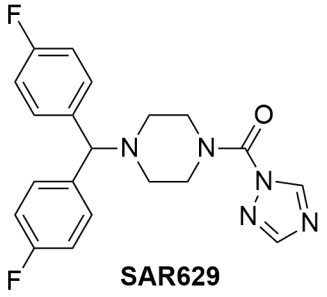

SAR629
IC_{50} = 1.1 nM

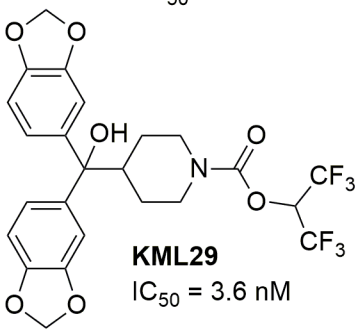

KML29
IC_{50} = 3.6 nM

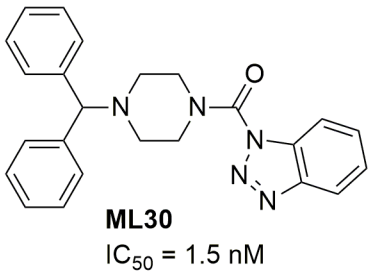

ML30
IC_{50} = 1.5 nM

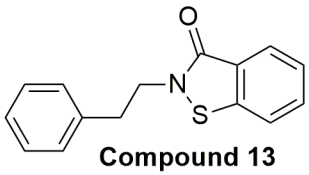

Compound 13
IC_{50} = 34.1 nM

cbdd_13751_f1.tif

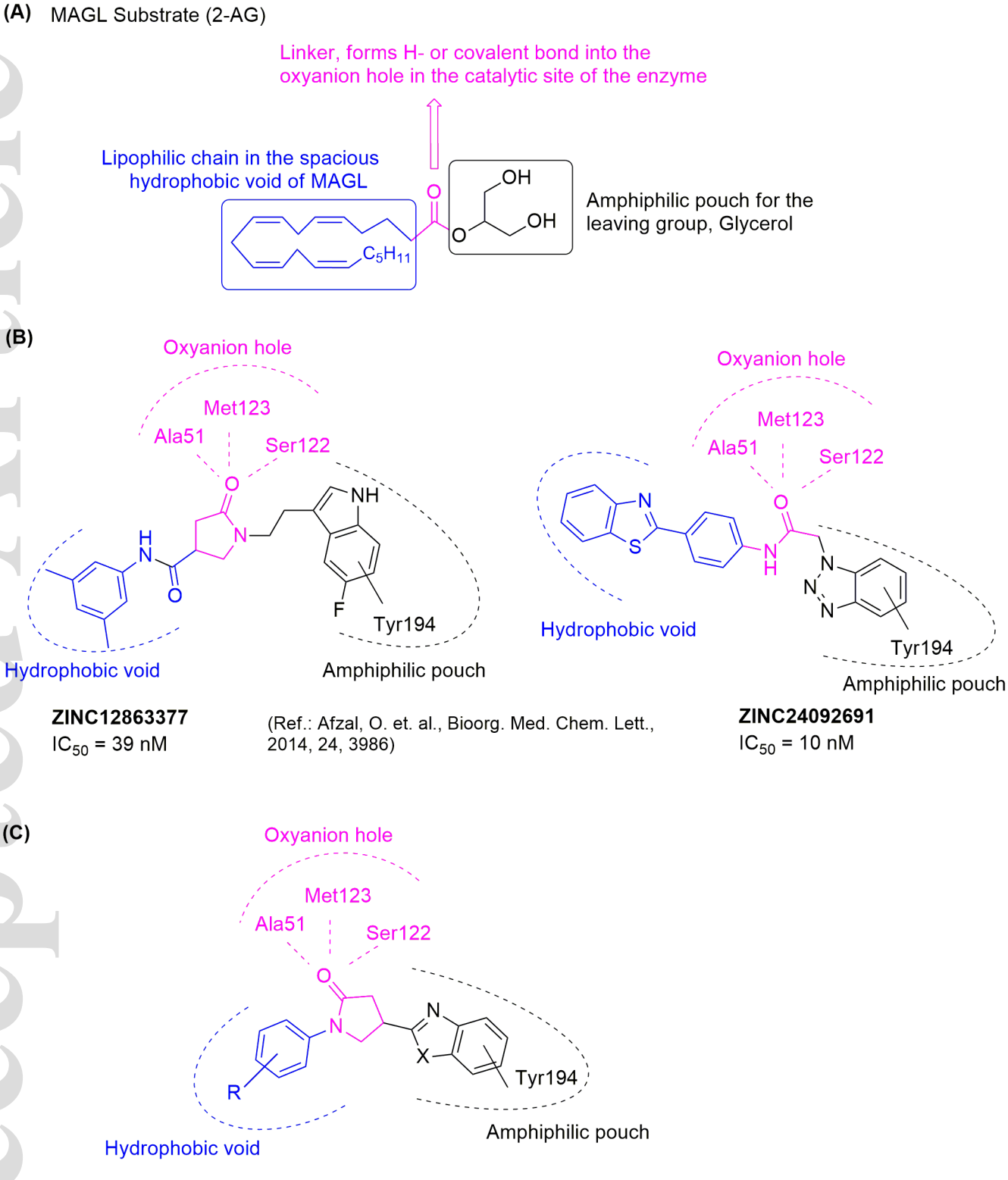

cbdd_13751_f2.tif

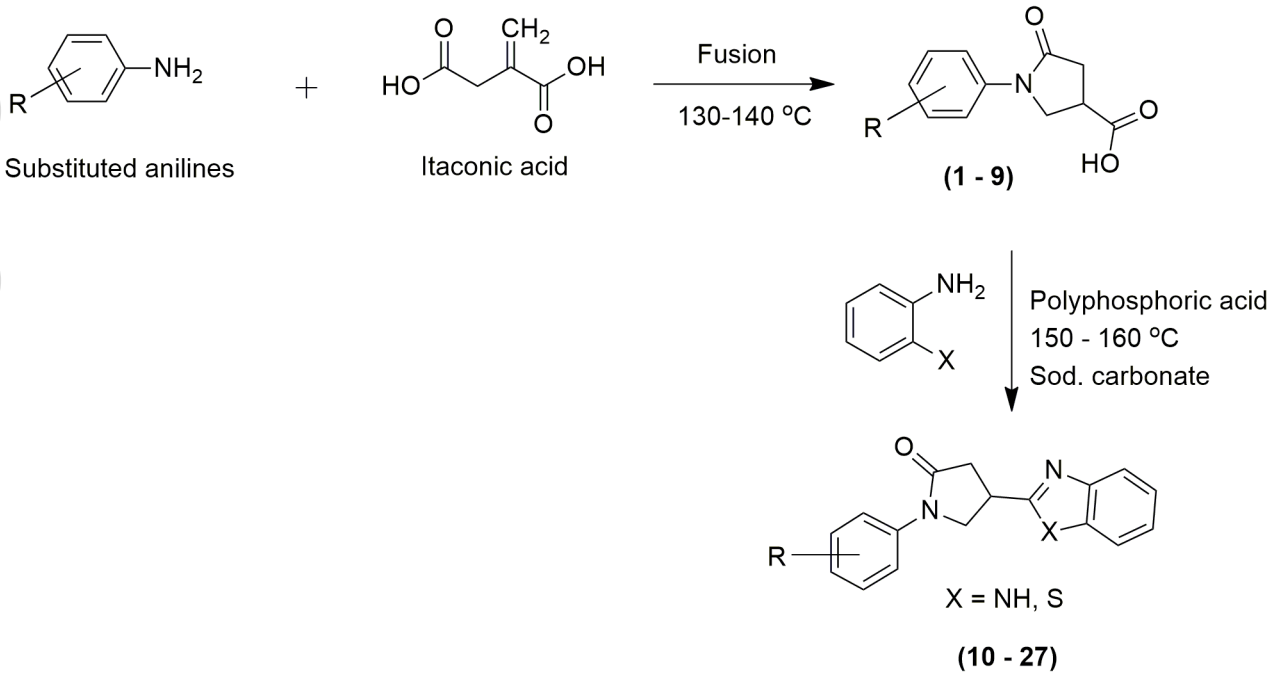

cbdd_13751_f3.tif

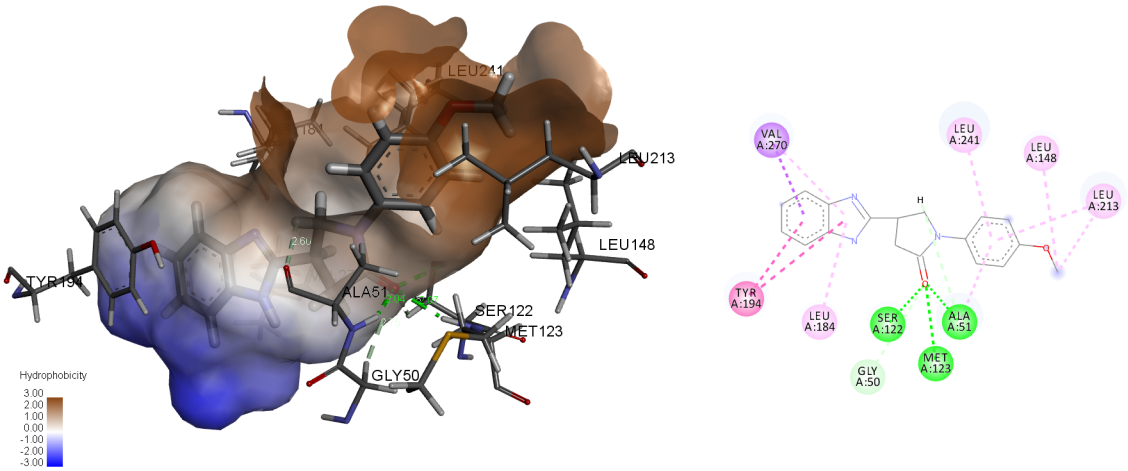

cbdd_13751_f4.tiff

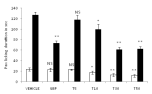

cbdd_13751_f5.tif